Endohedral Filling Effects in Sorted and Polymer-Wrapped Single-Wall Carbon Nanotubes

Han Li,* Georgy Gordeev, Dimitrios Toroz, Devis Di Tommaso, Stephanie Reich, and Benjamin S. Flavel*

ABSTRACT: Widespread use of the polymer extraction method for single wall carbon nanotubes (SWCNTs) and the ability of endohedral functionalization to alter their material properties make it important to examine the effect of filling on the separation result. Rate zonal centrifugation is used to obtain empty, water filled and perfluorooctane filled large (~1.45 nm), and single chirality small (~0.78 nm) diameter SWCNTs. These are transferred from water to toluene by dispersion with poly[(9,9 dioctylfluorenyl 2,7 diyl) *alt co* (6,6′ (2,2′ bipyridine))] (PFO BPy), and absorption and Raman spectroscopy are used to follow the extent of endohedral filling at each step. Measurements are made before and after centrifugation (supernatant) but also in the pellet. PFO BPy is found to stabilize endohedral functionalized SWCNTs in the supernatant, but a clear preference for less filled or empty species is shown. Molecular dynamics simulations are used to model the absorption spectrum of encapsulated water molecules in the PFO BPy/SWCNT/toluene system and explain why partial water filling is difficult to directly measure. These findings are then used to interpret separation results obtained for raw soot (without intentional filling) and with a view to the low yield of polymer based SWCNT extraction.

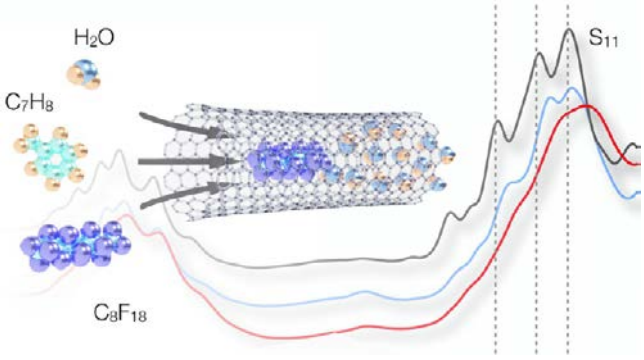

INTRODUCTION

Single wall carbon nanotubes (SWCNTs) have a one dimen sional (1D) hollow structure[1] that makes them the ideal nanometer scale container for molecules. Over the past few decades, fullerenes,[2,3] water or organic molecules,[4−6] 1D chains like nanowires and alkanes,[7−10] proteins and peptide amphiphiles,[11,12] catalysts,[13] and different dye molecules[14−17] have all been encapsulated within these small carbon cylinders.[18] Endohedral functionalization has allowed for the study of energy transfer processes in the case of dye molecules,[15,19] but it has also led to the emergence of new material properties. For example, nanoconfined water has been shown to form 1D single file chains in small diameter (d_t < 1 nm)[20−22] SWCNTs and ordered stacked polygonal rings in large diameter (d_t = 1−1.5 nm) ones.[23] These unique structures give rise to shifted phase boundaries and transitions,[20,24,25] enhanced water flow,[26−28] and novel dielectric properties.[29,30] Velioğlu et al.[31] recently showed that the water transport through SWCNTs of similar diameters strongly correlates to their metallicity, where semiconducting species constitute a lower obstruction for water entrance and exit than their metallic counterparts. Additionally, single chirality (9,8) SWCNTs showed an extraordinarily high water flux due to them possessing the lowest confinement energy.[31] Likewise in (9,8), Mikami et al.[29] used classical molecular dynamics (MD) calculations to suggest that so called "ice nanotubes" formed at low temperature consist of pentagonal water rings, which should lead to proton ordered phases along the SWCNT axis, and that these would give rise to ferroelectricity in water.

Beside techniques that provide a direct measurement of endohedral functionalization like nuclear magnetic resonance (NMR)[32] or X ray diffraction (XRD),[33] it is common to evaluate SWCNT filling by monitoring changes in their optical properties. More specifically, the positions of absorption[10] and photoluminescence[4] maxima as well as a hardening of the radial breathing mode (RBM) in resonance Raman spectra[25] confirm encapsulation. These techniques are accessible to most researchers and allow for the rapid analysis of energy transfer[15] and mechanical interactions[19] within SWCNT/filler com plexes, but they are also convenient to follow separation procedures and variations in the result that may arise due to the internal dielectric environment.[5,34] Recently Li et al.[35]

demonstrated that alkane filling can improve the resolution of the aqueous two phase extraction (ATPE) method, particularly for the separation of single chirality SWCNTs in the large diameter regime. This was surprising because all previous investigations combining endohedral filling and aqueous separation had shown encapsulation to have little effect on the result.[10,15,16,19,21,35,36] Likewise, van Bezouw et al.[15] and Campo et al.[10] used polymers to disperse filled SWCNTs in toluene and reported encapsulation to have no effect on the result. However, to be fair, these claims extend to confirming that sorted semiconducting SWCNTs were obtained and that these are now filled. Little is known about the effect of filled SWCNTs versus unfilled SWCNTs and/or raw soot on the extraction process nor have attempts been made to quantify the extent of filling after extraction. Certainly, due to the high solubility of the alkane or dye molecule in the surrounding organic solvent, this is a difficult process to follow. Never theless, taking into account that the polymer extraction method is probably now the most convenient technique to obtain semiconducting SWCNTs[37−41] with device relevant purity,[42−46] it is important to consider that endohedral filling may also alter the extraction result, especially since the method currently suffers from unexplainable low yields and when the result of extraction is strongly batch dependent.[47,48] To this end, we use aqueous based techniques to prepare small and large diameter SWCNTs that are either empty, water filled, or alkane filled and use these as a pseudo raw soot for polymer extraction. The separation result of samples with a highly uniform endohedral environment allows us to understand "real world" extractions using raw soot.

METHODS

Endohedral Filling of SWCNTs. As previously reported,[35] electric arc [EA AP (lot no. AP A264), Carbon Solutions] SWCNTs containing both open and close ended tubes were used to prepare empty and water filled SWCNTs (empty EA and H_2O@EA). To fill SWCNTs with perfluorooctane (C_8F_{18}@EA), EA P2 (lot no. 02 A011, Carbon Solution) SWCNTs (40 mg) were mixed with 3 mL of C_8F_{18} (98%, Sigma Aldrich) and incubated for 1 h. The filled SWCNTs were filtered (nylon membrane, 0.2 μm pore size) and washed with heptane (>99%, EMPLURA) to remove the C_8F_{18} outside.[10] The filter cake was then placed in a fume hood at room temperature to allow the heptane to evaporate before the further dispersion with surfactants. For the experiments with small diameter SWCNTs, 80 mg of CoMoCAT SG65i (lot no. SG65i L58) was heated in a tube furnace at 800 °C in vacuum for 1 h in order to ensure complete opening of the nanotubes.

Aqueous Suspension and Rate-Zonal Centrifugation. The preparation of aqueous SWCNT suspensions and rate zonal centrifugation have been extensively described in prior work.[10,35] In short, SWCNT suspensions were prepared by dispersing the SWCNT powders (40 mg) in 40 mL of 2% sodium deoxycholate (DOC) (20 g/L, BioXtra 98+%) by sonication for 45 min (tip, 0.9 W/mL) in an ice bath followed by centrifugation (45 560*g*, Beckman Optima L 80 XP, SW 40 Ti rotor) for 1 h. Eighty percent of the supernatant was collected and used for rate zonal centrifugation. Approximately 8 mL aliquots of the supernatant were then layered on top of 28 mL of 11% (volume/volume) iodixanol with 1% DOC (10 g/L) and centrifuged (2 h and 45 min for the arc tubes, 3 h and 15 min for the CoMoCAT tubes) in a VTi 50 rotor (Beckman Coulter) at 5240 rad/s (50 000 rpm) at 20 °C. The bands containing well individualized tubes were collected; see Figure S1. For EA AP SWCNTs, two bands were shown in the middle of each centrifuge tube with the top band containing empty EA and lower band containing H_2O@EA as shown previously.[21] Each of the different SWCNTs were finally concentrated and adjusted to 1% DOC (10 g/L) in a pressurized ultrafiltration stirred cell (Millipore) with a 300 kDa molecular weight cutoff membrane.

Polymer-Wrapped SWCNTs. Using a method previously reported,[41,49] the SWCNT samples were transferred from aqueous solution to toluene. SWCNTs (suspended in 1% DOC, after rate zonal centrifugation) were filtered onto a nylon membrane (0.2 μm pore size), and then washed with copious amounts of water to remove the DOC on the SWCNT surface. Approximately 100 mL of acetone (>99%, Sigma Aldrich) was used to wash the SWCNT film five times in order to remove external water. Subsequently, a similar wash step was performed with 100 mL of toluene (99.5%, ACS reagent, Sigma Aldrich) to remove the residual acetone and establish the toluene environment. Finally, 50 mL of anhydrous toluene (99.8%, Sigma Aldrich) was used to wash the film three times. The powders (0.5−1 mg) were then dispersed in 1−2 mL of anhydrous toluene with 1 mg/mL poly[(9,9 dioctylfluorenyl 2,7 diyl) *alt co* (6,6′ (2,2′ bipyridine))] (PFO BPy) by tip sonication for 30 min in an ice bath. Centrifugation was performed at 40 000*g* for 1 h (Beckman Optima MAX E, TLA 55 rotor). The sonicated suspension, pellets, and supernatants were collected for further spectroscopic characterizations.

Spectroscopy. UV−vis−NIR absorbance spectra were collected on a Cary 500 spectrometer from 1880 to 200 nm for samples in H_2O and from 3000 to 200 nm for samples in toluene in 1 nm increments through a 1 mm glass cuvette. Raman spectra were taken with a Renishaw InVia Reflex confocal Raman spectrometer using a laser energy of 2.33 eV (532 nm) under a 20× objective. The RBM shifts for each chirality were identified according to Araujo et at.[50] The nanotubes belonging to the $2n + m = 35$ laola family[51] were found in all samples and were used for analysis. First, the empty EA sample was fitted for all four conditions as shown in Figure S2. Each (n,m) chirality was represented by a Lorentzian line shape with equally set widths. The fitting function containing the same number of peaks was then applied to the filled samples. The resulted Raman shifts from the fit are summarized in Table S1 and plotted in Figure 3b.

CoMoCAT samples were excited in resonance with the (6,5) nanotube at the 2.2 eV laser line from a Radiant Dyes laser. R6G molecules dissolved in ethylene glycol were used as the active medium. The light was focused with a 100× (0.9 N.A.) objective on the sample. The backscattered light was passed through a long pass filter to remove Rayleigh light and was focused on a Horiba t64000 spectrometer slit functioning in single detection mode. The Raman (photoluminescence) light was dispersed by a 900 (600) grooves/mm grating and was detected with a silicon charge coupled device. In the raw CoMoCAT sample we found a single symmetric RBM peak belonging to unfilled (6,5) SWCNTs, whereas in the H_2O@(6,5) sample this peak was accompanied by an additional upshifted peak, corresponding to filled SWCNTs. In similar fashion we analyzed the photoluminescence (PL) spectra and found a single symmetric PL peak in the raw CoMoCAT sample and two peaks in the H_2O@(6,5) sample. To fit these, we fixed the parameters of the unfilled peak and left the parameters of the filled peak free. The root sum square

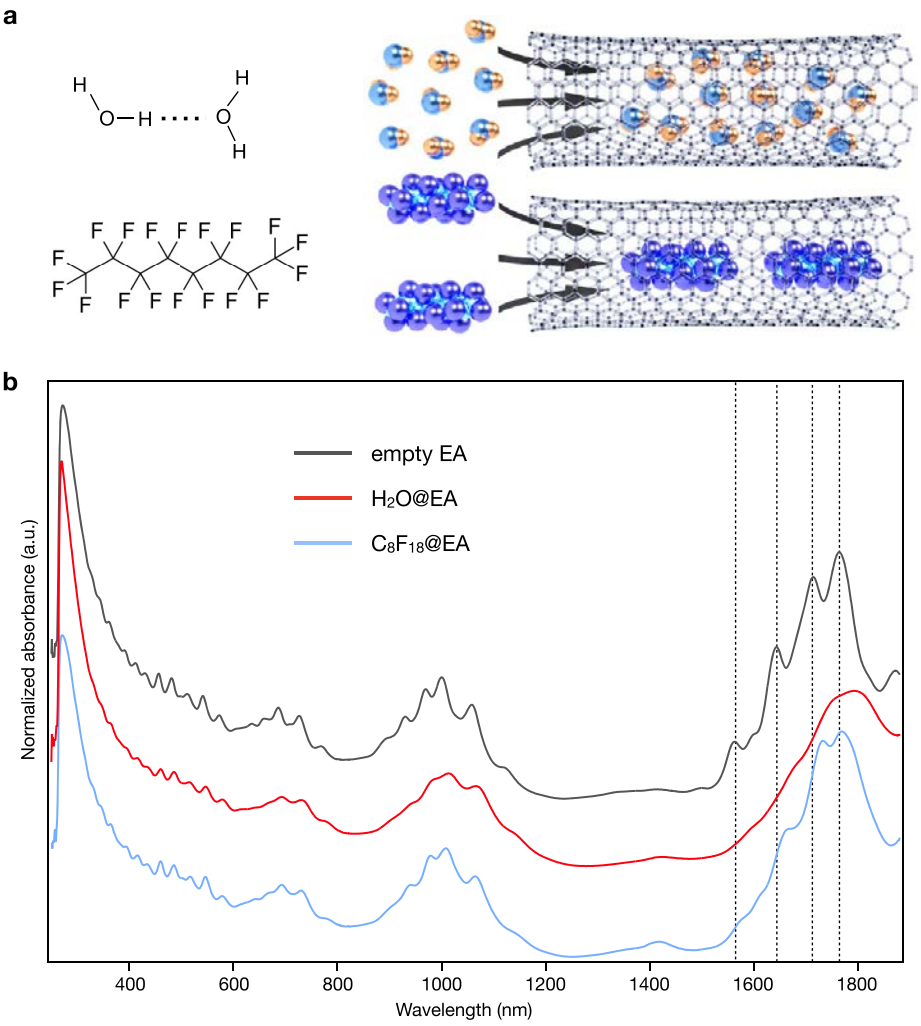

Figure 1. (a) Schematic illustration of water filled (H_2O@EA) and perfluorooctane filled (C_8F_{18}@EA) SWCNTs. (b) Absorption spectra of empty EA, H_2O@EA, and C_8F_{18}@EA SWCNTs after rate zonal centrifugation. All samples are dispersed in 1% sodium deoxycholate (DOC) in water, and all spectra are normalized at 270 nm with vertical offset for better comparison.

method was used to estimate the total RBM frequency measurement error; this includes statistical and systematic contributions. Statistical error represents standard deviation, calculated using multiple different Raman spectra acquired from the same sample. The systematic error is obtained using peak o mat software for a given model. The total error associated with each chirality is shown in Table S2.

Molecular Dynamics Simulation. All the simulations were conducted with the molecular dynamics suite Gromacs.[52] The initial models of the SWCNTs either with only water or with water and toluene inserted were constructed with the Packmol package for building initial configurations for molecular dynamics simulations.[53] The carbon nanotube atoms and the toluene atoms were treated with the general Amber force field.[54] The electrostatic potential was calculated based on the restrained electrostatic potential method.[55] The water molecules were characterized with a flexible variant of the TIP4P/2005 model of water.[56] The initial configurations created were equilibrated for 2 ns. We obtained well convergent velocity autocorrelation function profiles by using multiple time origins and overlapping intervals $[0, t]$ of time length equal to 10 ps with a very small time step of 0.1 fs. The spectrum density of states of the system was then computed with the g velacc tool within Gromacs. We applied periodic boundary conditions along the x and y axes. But along the z axis, which corresponded to the axis of the SWCNT, we placed two reflective walls at both ends of the SWCNT to maintain the solvent molecules (water or toluene) within the carbon nanotube. Details of the systems considered in this study (number of water and toluene molecules, number of the carbon atoms constituting the nanotube, and dimension of the simulation cell solution concentrations) are reported in Table S3.

RESULTS AND DISCUSSION

Electric arc discharge (EA) SWCNTs were first investigated because the raw soot contains a mixture of open (able to be filled) and closed (empty) species, which through rate zonal centrifugation can be isolated and which provide clear control samples for the effects of endohedral filling. In this work, water (H_2O@EA) and perfluorooctane (C_8F_{18}@EA) were used as fillers because they are insoluble in toluene. Spectra pertaining to the preparation of empty, H_2O filled, and C_8F_{18} filled samples with rate zonal centrifugation can be found in Figure S1. EA SWCNTs have an average diameter of 1.45 nm, and it is expected that the small H_2O molecules will form clusters interconnected by hydrogen bonds[21,57,58] while the larger C_8F_{18} molecules will arrange in a 1D single file;[15] see Figure

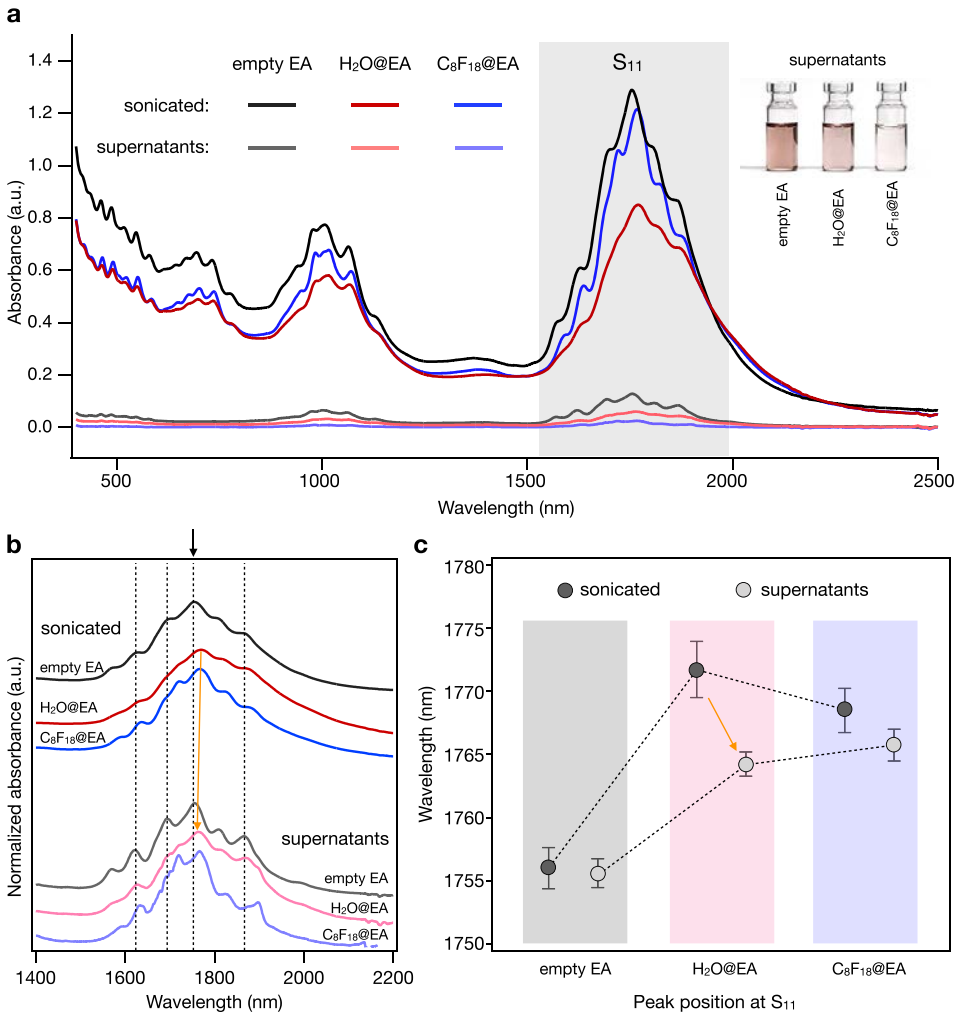

Figure 2. (a) Absorption spectra of empty EA (black), H_2O@EA (red), and C_8F_{18}@EA (blue) samples dispersed by PFO BPy in toluene before (sonicated) and after (supernatant) centrifugation. A photograph of the supernatant for each sample is shown as an inset. (b) Enlarged view of the S_{11} region before and after centrifugation. Dashed lines indicate the main peaks that can be identified, and a vertical offset is made to aid comparison. (c) The peak at ~1755 nm [closest to the S_{11} of (16,3)] is chosen to compare the spectral shift before and after centrifugation for the different fillers.

1a. An absorption spectrum of each sample after isolation is shown in Figure 1b. The filling with C_8F_{18} was not found to significantly alter the overall absorption spectrum of the SWCNTs. EA SWCNTs have their first (S_{11}), second (S_{22}), and third (S_{33}) semiconducting optical transitions located in the spectral ranges of 1500−2000, 800−1200, and 400−600 nm, respectively. Filling of the SWCNTs is immediately visible upon examination of their S_{11} spectral features. In agreement with Campo et al.[10,59] the S_{11} peaks of empty EA SWCNTs are clearly sharper and narrower than those of H_2O@EA and C_8F_{18}@EA. Compared to C_8F_{18}@EA, the H_2O@EA sample exhibits a broad and almost single peak at S_{11}, without any easily identifiable structure. Furthermore, as indicated by the black dashed lines, the S_{11} peaks of H_2O@EA and C_8F_{18}@EA are red shifted (by up to 30 nm) relative to the empty EA sample, and this is another important verification of successful filling.[10,59] This is equivalent to a ΔE_{11} of ~10 meV. ΔE_{22} and ΔE_{33} were estimated to be ~16 and 20−26 meV, respectively.

The π plasmon peak (270 nm) was used to estimate the concentration of each sample, and the same amount of the three types of SWCNTs was filtered, washed, and resuspended in toluene with PFO BPy. The use of PFO BPy and the centrifugation conditions later employed were chosen to be representative of a typical polymer extraction process found in the literature.[48] Absorption spectra of the dispersions directly after sonication are shown in Figure 2a. The trend in spectral features across all three samples (peak position/broadness) is similar to that of Figure 1b and suggests that the endohedral filler was well preserved during the transfer process from aqueous to organic solvent. After centrifugation (40 000g/1 h) the supernatants from empty EA, H_2O@EA, and C_8F_{18}@EA, respectively, were collected, and absorption spectra of these are also shown in Figure 2a. Comparison of the sonicated to centrifuged spectra reveals that the endohedral filler had an effect on the yield of semiconducting SWCNT extraction. Likewise, a difference in yield can be seen in a photograph of the supernatants provided as an inset to Figure 2a. The yield estimated from the S_{11} peak area was empty EA > H_2O@EA > C_8F_{18}@EA. An explanation for this difference is related to the density of the filled SWCNT/polymer complex and is in agreement with work by Campo et al. on different types of filled SWCNTs in aqueous solutions.[10] Using analytical ultracentrifugation (AUC) they measured the sedimentation coefficient distribution of empty, water filled, and C_8F_{18} filled

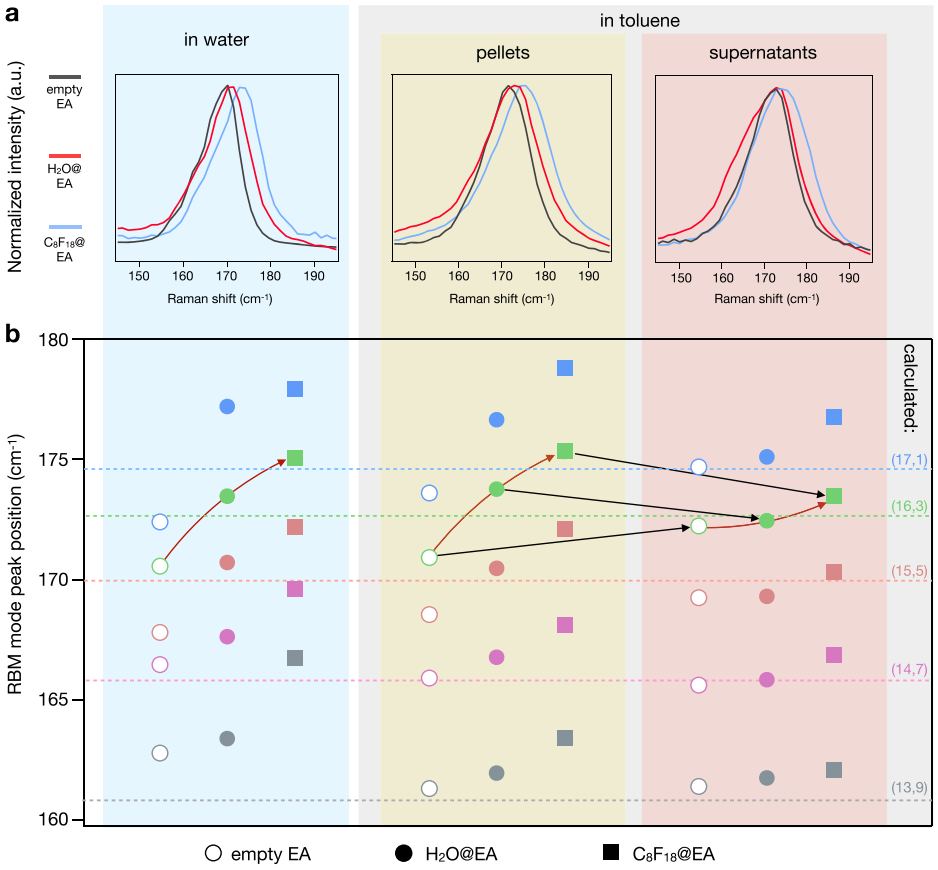

Figure 3. (a) Resonant Raman spectra measured with 532 nm excitation of the empty EA (black), H_2O@EA (red), and C_8F_{18}@EA (blue) samples dispersed in water along with the pellet and supernatant after transfer to toluene using PFO BPy. (b) RBM peak positions of (17,1), (16,3), (15,5), (14,7), and (13,9) compared to the calculated value obtained from Araujo et al. (ref 50) (dashed line). The five (n,m) species are indicated by different colours for the empty (open circle), H_2O@EA (solid circle) and C8F18@EA (solid square) samples. The black arrows indicate the shift direction from the pellet to the supernatants, and the red arrows highlight the shifts due to the different fillings.

EA SWCNTs in aqueous solutions and showed that C_8F_{18}@EA > H_2O@EA > empty EA for both anhydrous and hydrated buoyant densities.[10,60] A similar trend is expected in toluene with PFO BPy. For reference, the densities of the individual components used in this work are C_8F_{18} (1.77 g/cm^3) > SWCNTs (1.2−1.5 g/cm^3) > H_2O (0.998 g/cm^3) > toluene (0.867 g/cm^3) > air/empty (0.0012 g/cm^3) > vacuum/empty.

Figure 2b shows an enlargement of the S_{11} region before and after centrifugation of the three samples. As expected, the peaks become sharper after centrifugation due to the removal of bundles, but in general, across the three samples the trend in peak shape and position remains unchanged. This once again confirms that each sample is endohedral filled with something different, but examination of spectra before and after centrifugation now begin to show spectral shifts, and these reveal possible changes in the extent of filling. This is most clear for the H_2O@EA sample, which shows a clear blue shift (3−6 nm) for most of the peaks that can be identified. These are marked by dashed lines in Figure 2b. The empty EA and C_8F_{18}@EA peak positions are not obviously changed after centrifugation and are all within ±1 nm of their original value. This is at the resolution of our spectrometer. In Figure 2c a specific comparison is made by examining the peak most likely associated with (16,3) at ∼1755 nm. For the H_2O@EA sample a 6 nm blue shift is obtained after centrifugation, whereas the same peak for the empty EA and C_8F_{18}@EA samples is only slightly red shifted (1 nm) and blue shifted (1 nm), respectively. Under the assumption that S_{11} of endohedral filled SWCNTs is red shifted compared to the empty case, it is possible to speculate that a blue shift for the supernatant of the C_8F_{18} and H_2O samples means that those SWCNTs which remain suspended in the supernatant are comparatively less filled than those in suspension prior to centrifugation. The small red shift for the empty EA SWCNTs may be an indication that they have become partially opened during redispersion and are now filled with toluene; however, tightly bound PFO BPy is the most likely origin.[51]

In order to further investigate the extent of endohedral filling after centrifugation, resonant Raman measurements were performed on the three different samples. Figure 3a compares RBM spectra for the dispersions in water to those of the supernatant and pellet obtained after centrifugation in toluene. For the samples dispersed in water the RBM peak positions were 170.1 cm^{-1} (empty), 171.5 cm^{-1} (H_2O filled), and 172.8 cm^{-1} (C_8F_{18} filled). An upshift due to endohedral filling is in good agreement with previous work from Campo et al.[10] and Streit et al.[19] and indicates a change in hardness of the filled SWCNTs. The small size and compressibility of the H_2O molecules compared to C_8F_{18} means that this effect is greatest for the C_8F_{18}@SWCNTs. A similar trend across the samples for both the pellet and supernatant once again suggests that each has a different filler. This was observed for multiple samples and laser positions; see Figure S2. However, in order to observe the effect of centrifugation on the extent of

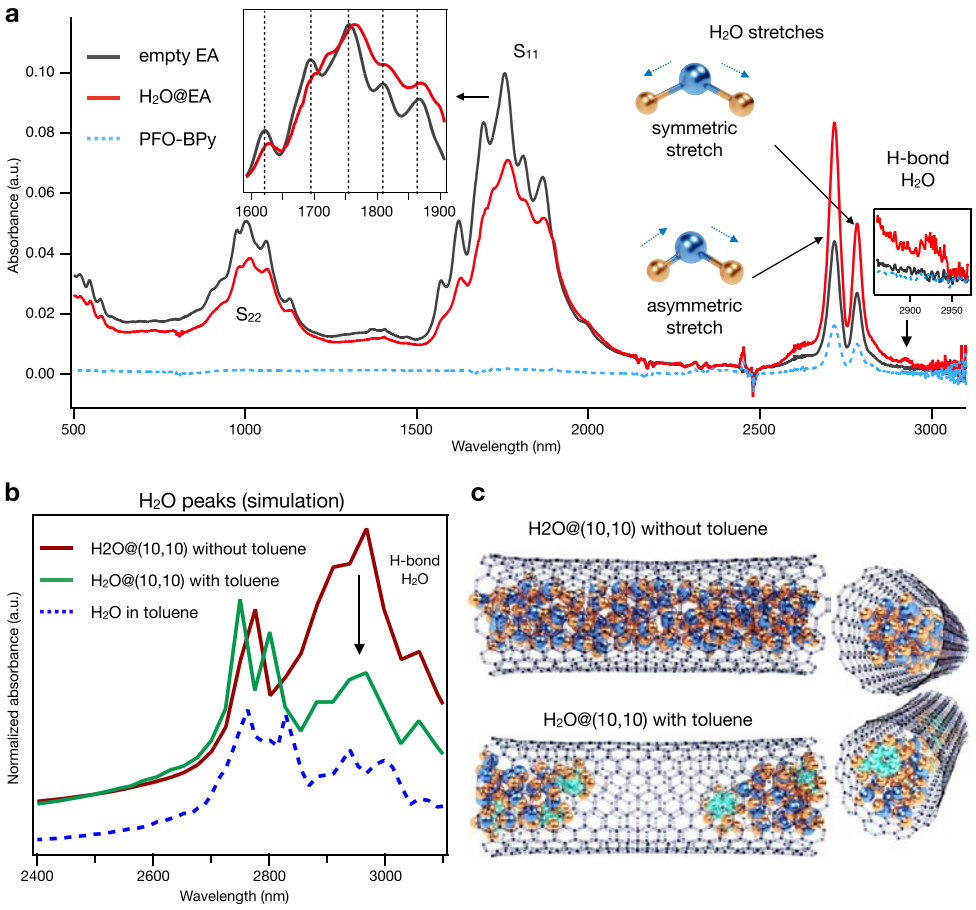

Figure 4. (a) Absorption spectra of the supernatants from empty EA and H_2O@EA SWCNTs in toluene. Water peaks can be identified between 2500 and 3000 nm. (b) Vibrational spectra of water computed from MD simulations of H_2O@(10,10). The solid green and red lines correspond to water inside the SWCNT with and without toluene, respectively; the dashed blue line corresponds to water in bulk liquid toluene. (c) End and side views of snapshots from MD simulations of H_2O@(10,10) with and without toluene.

endohedral filling it is instructive to look at the RBM peak position of individual (n,m) species within the EA SWCNT population. To achieve this, we used a fitting procedure on the RBM data. Figure 3b compares the RBM peak position of (17,1), (16,3), (15,5), (14,7), and (13,9), Figure S3 shows the fitted spectra, and Table S1 lists the associated peak positions. The (16,3) SWCNT will now be used as an example, but the same trend is seen for all chiralities considered. For the H_2O@EA sample the RBM position of (16,3) in the pellet (173.8 cm^{-1}) compared to the supernatant (172.5 cm^{-1}) shows a softening of the SWCNT and suggests that the SWCNTs in the supernatant are less filled than the pellet, and likewise for the C_8F_{18}@EA sample, which had pellet and supernatant peaks at 175.3 and 173.4 cm^{-1}, respectively. Alternatively, the supernatant (172.2 cm^{-1}) of the empty sample was hardened relative to the pellet (170.9 cm^{-1}) and is in good agreement with a tightly bound PFO Bpy layer. It is also in agreement with a polymer sorting process that prefers to disperse SWCNTs that are empty or only partially filled. The RBM positions of all chiralities in the supernatant, regardless of filling, approach a similar value that is marked by a dashed line [172.8 cm^{-1} for (16,3)] in Figure 3b and which happens to correspond to the theoretically calculated value from Araujo et al.[50] Essentially, this means that the supernatant is constituted of empty or partially filled nanotubes, whereas the pellet contains filled species. This is reflected in a broadening of the RBM envelope of the supernatants and a narrowing of the envelope associated with the pellet; see Figure S4. At this stage it is only possible to speculate on the reason for this preference, but we believe that there are two important factors: the overall polarizability of the SWCNT due to filling and density effects as already discussed. In density functional theory (DFT) calculations[61] and some experimental studies[38,48,62] it has been discussed that a contrast in the polarizability between metallic and semiconducting SWCNTs leads to the preferential dispersion of semiconducting species,[37] but in the future perhaps the explanation should be extended to include the inner and outer dielectric environment.

Absorption spectroscopy was used to further analyze the structure of water within the nanotubes after centrifugation. This is a unique measurement and unlike previous studies in solution where measurement of the water spectrum inside a nanotube was precluded by the surrounding solution. In Figure 4a, extended absorption spectra (400−3100 nm) are shown for the supernatants of empty and H_2O@EA dispersed by PFO BPy in toluene. In the wavelength range of 2500−3000 nm there are two clear peaks associated with the vibration of H_2O molecules. These are the asymmetric (2716 nm or 3682 cm^{-1}) and symmetric (2782 nm or 3594 cm^{-1}) stretching modes of water.[63] Unlike bulk water with strong intermolecular hydrogen bonding interactions, having water within a nano tube will lead to “free −OH” groups, and this will enhance the

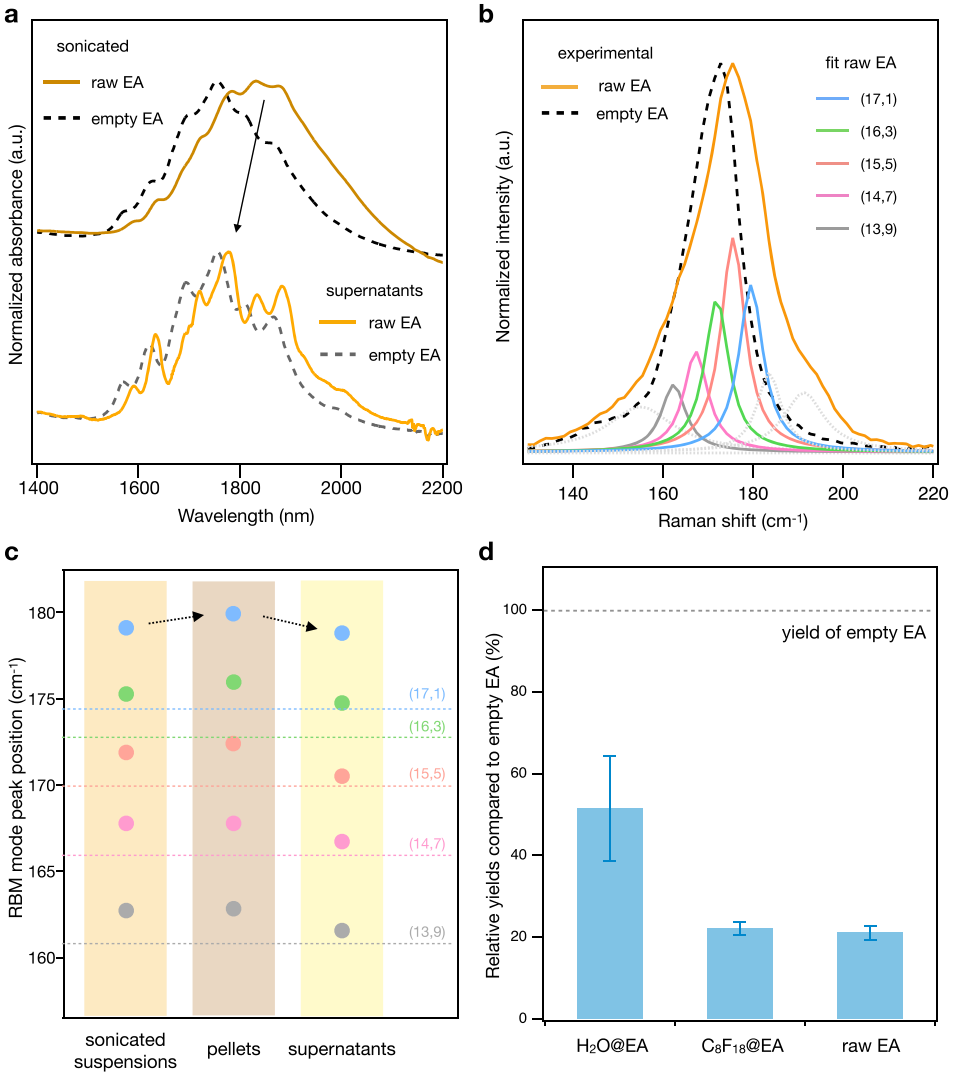

Figure 5. (a) Comparison of absorption spectra of raw EA soot and empty EA SWCNTs sonicated with PFO BPy in toluene before (sonicated) and after (supernatant) centrifugation. (b) Resonant Raman spectra measured with 532 nm excitation of the supernatant from raw EA (yellow solid line) and empty EA (black dashed line) samples. The fitted spectra for (17,1), (16,3), (15,5), (14,7), and (13,9) are shown as colored lines. (c) RBM peak shifts for the chiral species identified in panel b compared to the calculated value obtained from Araujo et al. (ref 50) (dashed line). (d) The relative yield of separation based on the endohedral filling (empty EA SWCNTs were set to a yield of 100%).

strength of these intramolecular stretches.[64,65] Many previous simulation and experimental studies point out that, when water is confined inside a SWCNT, it is difficult for water to hydrogen bond to itself[57,58,64,66] and that this is an effect observed not only for the relatively small diameter nanotubes (diameter ~0.6−0.8 nm), where a 1D single line structure of H_2O is expected,[21] but also for the larger diameter SWCNTs (≥1.4 nm) due to a water layer with dangling OH bonds facing the nanotube inner wall.[57] Although the spectral features of H_2O in this range are similar to those of previous works,[57,67] control experiments on the empty EA SWCNTs and also PFO BPy in toluene (without SWCNTs) show that these two peaks are apparently not only due to water inside the nanotube. Both the asymmetric and symmetric water stretches are also seen for the empty EA SWCNTs and PFO BPy in toluene. As anhydrous toluene was used for these experiments this means that water molecules have been introduced into the system during the experimental process, for example, during solvent exchange and sonication, and that these are now isolated in the toluene. However, it should be noted that the peak intensities of the water stretches for the H_2O@EA sample are larger than in the case of the two controls. Therefore, the "real" spectra of water filled inside the EA nanotubes is likely highly overlapped with the absorption of these "free" or clustered H_2O molecules in toluene or dangling OH bonds on the surface of SWCNTs. For large diameter SWCNTs it has also been shown that intermolecular interactions (particularly between H_2O rings within the SWCNT) lead to the formation a distorted hydrogen bonding network and that these result in the emergence of additional stretching modes.[64] However, the intensity of these modes is very weak, and more than half the intensity of the stretching vibrations will still come from intramolecular vibrations (discussed above), even for fully hydrated SWCNTs.[57] In the H_2O@EA sample, it is possible that such a distorted hydrogen bond network of water inside the EA tubes is visible at 2900−2950 nm (3420−3390 cm^{-1}),[64] and it is not seen in any of the controls. To confirm this hypothesis, we have computed through MD simulations the absorption spectra of water confined in a (10,10) nanotube, H_2O@(10,10) (diameter of 1.38 nm, close to that

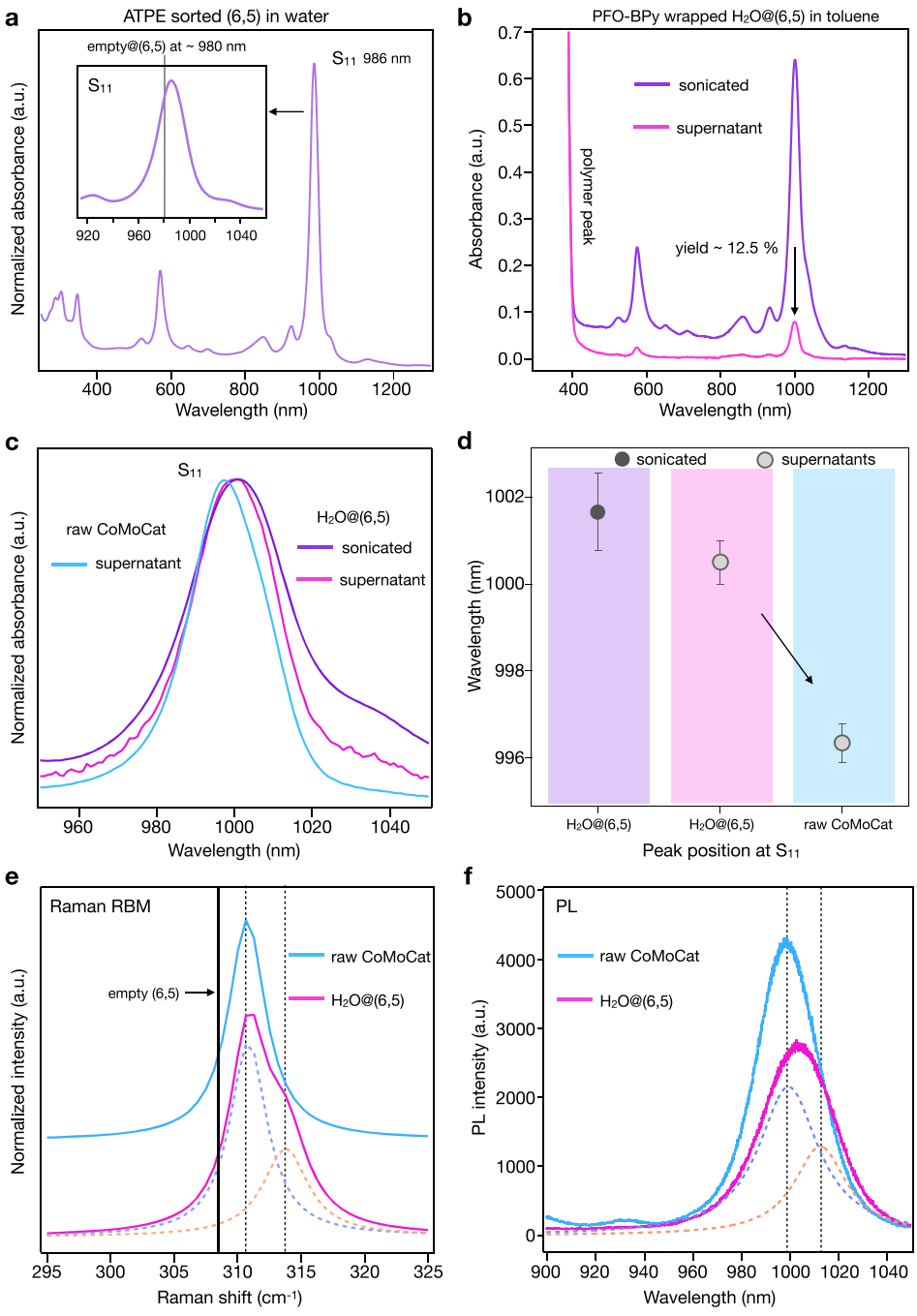

Figure 6. (a) Absorption spectrum of ATPE separated H_2O@(6,5) dispersed in water with 1% DOC. The inset compares the position of S_{11} to empty (6,5) from Ma et al. (ref 20). (b) H_2O@(6,5) dispersed by PFO BPy after transfer to toluene and before and after centrifugation. (c) Comparison of the S_{11} region of PFO BPy wrapped raw CoMoCAT to H_2O@(6,5) with (d) the peak position indicated before and after centrifugation. (e) Resonant Raman and (f) photoluminescence spectroscopy of the supernatant from raw CoMoCAT and H_2O@(6,5). The RBM position for empty (6,5) was obtained from Cambré et al. (ref 71).

of the EA soot) for the two cases of partial and complete water filling. Their spectra in Figure 4b are compared to that of a cluster of water molecules in pure toluene. In the case of partial filling, we placed toluene inside the nanotube to represent the possible solvent exchange with the endohedral environment in the H_2O@EA sample. Figure 4c gives a graphical representa tion of the two filling cases, with Figure S5 providing an enlarged view where an ordered ring of water forms within the (10,10) nanotube in the case of complete filling. The formation of such an ordered hydrogen bond network leads to the emergence of a broad absorption peak at 2800−3100 nm (Figure 4b, in red). These interactions are then reduced when the nanotube is partially filled with water or when the water structure is broken due to the inclusion of toluene within the nanotube. Consequently, the spectra of H_2O@(10,10) with toluene (Figure 4b, in green) and water clusters in pure toluene (Figure 4b, in blue) show very similar profiles because the absorption spectrum is defined by the existence of a water cluster. Interestingly, analysis of the MD simulations of H_2O@(10,10) shows that the mean square displacement of the water, which gives a measure of water mobility, is decreased by the presence in SWCNT of toluene (Figure

S6). The weak intensity of the intermolecular water peak in our samples compared to that of previous calculations and experimental results[67,68] suggests that it is difficult to maintain complete water upon transfer to an organic solvent, but it also explains why partial water filling in polymer based nanotube separations has until now mostly been neglected. Unless the SWCNTs are fully hydrated it is difficult to confirm the presence of endohedral water with absorption spectroscopy.

After studying uniformly filled SWCNTs we turn to the situation faced by most researchers,[69,70] namely, using PFO BPy to disperse and sort SWCNTs from a commercially available raw soot. In this case the endohedral state is mostly unknown (at least it is not stated by the manufacturer) and is variable. In the first example, raw SWCNTs of EA P2 (open ended,[10,35] carbonaceous purity >90%) were used. All other experimental conditions were held constant. In Figure 5a absorption spectra of the sonicated suspension (before centrifugation) and supernatant are compared to the empty EA SWCNTs from Figure 2b. In both cases, a clear red shift can be seen for the raw versus empty EA samples. A shift of ∼50 nm is due to a combination of other non nanotube contaminates in the raw soot, but it also indicates that the SWCNTs are filled. Raman measurements in Figure 5b suggest water filling with an upshift of 2.7 cm^{-1} seen for the supernatant of the raw versus the empty EA sample,[25,71,72] and this is probably a result of storage of the raw soot in ambient conditions. Once again, similar to the H_2O@EA and C_8F_{18}@EA cases, the chiral analysis in Figure 5c shows a downshift of the raw EA supernatants compared to the pellet and sonicated samples. These results should not be confused to mean that the raw EA soot is entirely water filled but rather that there is a partial filling. However, the polymer's preference to disperse unfilled or less filled SWCNTs will mean that this partial filling will have an impact on the final yield of separation. By integrating the area under the S_{11} region, a rough comparison of yield is shown in Figure 5d, where the empty EA supernatant with the highest concentration is set to 100% and the raw EA, H_2O@EA, and C_8F_{18}@EA samples are compared to it. It should be noted that the relative yields are only a very rough estimation given that there could be many non SWCNT impurities in the raw soot, and these make a direct comparison difficult.

The use of polymer wrapping to separate (6,5) from the CoMoCAT raw soot is arguably the more common use of PFO BPy within the scientific community,[39,44,48,49] and it is thus the second example we provide. The small diameter of (6,5) now prevents the ingress of toluene,[73] and a linear chain of water is obtained when filled.[21,57] Recently Qu et al. showed that *n* hexane and cyclohexane, which have kinetic diameters (KD) of ∼0.43 and ∼0.60 nm, respectively, can fit inside SWCNTs with a diameter of >0.78 nm,[73] whereas only *n* hexane is able to fit inside the next smallest species [(6,5) with d_t = 0.76 nm] by elongating its structure. Toluene has a KD of 0.585 nm[74] with a structure similar to that of cyclohexane, and thus it should behave similarly. The raw soot also does not contain an appreciable amount of empty (closed) SWCNTs, and experiments with perfluoroctane are not possible because it has a sieving diameter of ∼1 nm, which corresponds to (8,7).[59] ATPE was used to isolate H_2O@(6,5), and the absorption spectrum is shown in Figure 6a. Water filling resulted in a 6 nm red shift of S_{11} relative to the data provided by Ma et al.[20] for empty surfactant dispersed (6,5). Using the same transfer procedure as for the EA SWCNTs, around 0.05 mg of H_2O@(6,5) was redispersed in toluene with PFO BPy. Absorption spectra before and after centrifugation are shown in Figure 6b. Here, once again the presence of endohedral water appears to lead to a low yield (12.5%), and this is despite the high selectivity of PFO BPy for (6,5) and the fact that it was essentially the only chiral species in the material to be dispersed. In contrast to the EA SWCNT case in Figure 5, the use of a presorted fraction allows for the effect caused by non SWCNT related material or nonselected chiralities in the raw material to be neglected. Due to the lack of empty (6,5) as a control, the water filled case was compared to raw CoMoCAT soot. Parts c and d of Figure 6 compare the S_{11} region of these samples, where the supernatant (1000 nm) and sonicated (1001 nm) samples for the H_2O filled case can be seen to be red shifted relative to the raw soot (997 nm). Resonant Raman analysis in Figure 6e of the supernatants reveals two subpopulations for the H_2O@(6,5) sample. Cambré et al.[71] have provided a reference value for empty (6,5) dispersed by surfactants of around 308 cm^{-1}. In agreement with the EA SWCNTs, if PFO BPy wrapping imparts a 1−2 cm^{-1} shift relative to surfactant samples the two RBM modes for the H_2O@(6,5) samples can be assigned to (6,5) with water filling (313.8 cm^{-1}) and empty (310.7 cm^{-1}).[59] Here once again it is important to state that Qu et al.[73] recently showed that linear molecules present in trace amounts in the toluene can fill (6,5) and that these may also be associated with the peak at 310.7 cm^{-1}. The supernatant from the raw soot was found to only contain the peak at 310.7 cm^{-1}. Considering how widespread the use of polymer wrapped SWCNTs is in optoelectronic,[75,76] photovoltaic,[42,47,61] and transistor devices[44] this is an important finding because control of the endohedral environment will not only assist improvements in device performance in the future but also extraction yield. An example of this is shown in Figure 6f where the PL spectra of polymer wrapped (6,5) from raw and water filled CoMoCAT are compared. In addition to a 14 nm blue shift the PL intensity of the less filled case is higher than that of the more heavily water filled case. Processing improvements for CNT based devices will therefore not only come by focusing on reduced chirality dispersions[47,77] and/or removing excess polymer[78−80] but also by controlling the endohedral environment of the raw material used.

CONCLUSION

SWCNTs with uniform and controlled endohedral functionalization (empty, H_2O, and C_8F_{18}) were prepared and characterized in both aqueous and organic suspensions. It was shown that PFO BPy is capable of dispersing endohedral filled SWCNTs and that the yield of dispersion is strongly coupled to the extent of filling. In general, the supernatant was found contain SWCNTs that were weakly filled, and the highest yield was obtained for empty species. In light of this, the explanation of a low yield of (6,5) extraction from CoMoCAT appears to be simple: there are simply very few empty/closed SWCNTs in the raw soot to be extracted. It is clear that efforts to control the endohedral environment prior to separation will lead to better device performance and higher extraction yields but also continued development of nanotube growth processes with particular emphasis on the obtainment of end capped species in the raw soot will be important. The dispersion of SWCNTs will always remain a balancing act between their destruction and individualization, but just as the gentler shear force mixing approach has resulted in higher

yields compared to sonication, so too will an increase in the number of close ended species in the raw material to be dispersed by the polymer.

AUTHOR INFORMATION

Corresponding Authors

Han Li − *Institute of Nanotechnology, Karlsruhe Institute of Technology, 76344 Eggenstein Leopoldshafen, Germany*; Email: han.li@kit.edu

Benjamin S. Flavel − *Institute of Nanotechnology, Karlsruhe Institute of Technology, 76344 Eggenstein Leopoldshafen, Germany;* Email: benjamin.flavel@kit.edu

Authors

Georgy Gordeev − *Department of Physics, Freie Universität Berlin, 14195 Berlin, Germany;*

Dimitrios Toroz − *School of Biological and Chemical Sciences, Materials Research Institute, Thomas Young Centre, Queen Mary University of London, London E1 4NS, United Kingdom*

Devis Di Tommaso − *School of Biological and Chemical Sciences, Materials Research Institute, Thomas Young Centre, Queen Mary University of London, London E1 4NS, United Kingdom;*

Stephanie Reich − *Department of Physics, Freie Universität Berlin, 14195 Berlin, Germany;*

Author Contributions

H.L. and B.S.F. conceived the idea for this work and designed the experiments. Molecular dynamic simulation was performed by D.T. and D.D.T. G.G. and S.R. characterized the samples with Raman spectroscopy. All authors contributed to the preparation of the manuscript.

Notes

The authors declare no competing financial interest.

ACKNOWLEDGMENTS

B.S.F. and H.L. gratefully acknowledge support from the Deutsche Forschungsgemeinschaft (DFG) under Grant Nos. FL 834/2 1, FL 834/2 2, FL 834/5 1, and FL 834/7 1. D.T. and D.D.T. gratefully acknowledge the ACT programme (Horizon 2020 no. 294766) for financial support and the U.K. MMM Hub (EP/P020194/1), HEC MCC (EP/L000202, EP/R029431), and Queen Mary's Research IT for computing resources.

REFERENCES

(1) Iijima, S.; Ichihashi, T. Single Shell Carbon Nanotubes of 1 nm Diameter. *Nature* **1993**, *363*, 603−605.

(2) Smith, B. W.; Monthioux, M.; Luzzi, D. E. Encapsulated C_{60} in Carbon Nanotubes. *Nature* **1998**, *396*, 323−324.

(3) Liu, X.; Pichler, T.; Knupfer, M.; Golden, M.; Fink, J.; Kataura, H.; Achiba, Y.; Hirahara, K.; Iijima, S. Filling Factors, Structural, and Electronic Properties of C_{60} Molecules in Single Wall Carbon Nanotubes. *Phys. Rev. B: Condens. Matter Mater. Phys.* **2002**, *65*, 045419.

(4) Chiashi, S.; Hanashima, T.; Mitobe, R.; Nagatsu, K.; Yamamoto, T.; Homma, Y. Water Encapsulation Control in Individual Single Walled Carbon Nanotubes by Laser Irradiation. *J. Phys. Chem. Lett.* **2014**, *5*, 408−412.

(5) Khlobystov, A. N.; Britz, D. A.; Briggs, G. A. D. Molecules in Carbon Nanotubes. *Acc. Chem. Res.* **2005**, *38*, 901−909.

(6) Li, L. J.; Khlobystov, A.; Wiltshire, J.; Briggs, G.; Nicholas, R. Diameter Selective Encapsulation of Metallocenes in Single Walled Carbon Nanotubes. *Nat. Mater.* **2005**, *4*, 481−485.

(7) Kitaura, R.; Imazu, N.; Kobayashi, K.; Shinohara, H. Fabrication of Metal Nanowires in Carbon Nanotubes Via Versatile Nano Template Reaction. *Nano Lett.* **2008**, *8*, 693−699.

(8) Jankovic, L.; Gournis, D.; Trikalitis, P. N.; Arfaoui, I.; Cren, T.; Rudolf, P.; Sage, M. H.; Palstra, T. T.; Kooi, B.; De Hosson, J.; et al. Carbon Nanotubes Encapsulating Superconducting Single Crystalline Tin Nanowires. *Nano Lett.* **2006**, *6*, 1131−1135.

(9) Shi, L.; Rohringer, P.; Suenaga, K.; Niimi, Y.; Kotakoski, J.; Meyer, J. C.; Peterlik, H.; Wanko, M.; Cahangirov, S.; Rubio, A.; et al. Confined Linear Carbon Chains as a Route to Bulk Carbyne. *Nat. Mater.* **2016**, *15*, 634−639.

(10) Campo, J.; Piao, Y.; Lam, S.; Stafford, C. M.; Streit, J. K.; Simpson, J. R.; Hight Walker, A. H.; Fagan, J. A. Enhancing Single Wall Carbon Nanotube Properties through Controlled Endohedral Filling. *Nanoscale Horiz.* **2016**, *1*, 317−324.

(11) Kang, Y.; Liu, Y. C.; Wang, Q.; Shen, J. W.; Wu, T.; Guan, W. J. On the Spontaneous Encapsulation of Proteins in Carbon Nanotubes. *Biomaterials* **2009**, *30*, 2807−2815.

(12) Arnold, M. S.; Guler, M. O.; Hersam, M. C.; Stupp, S. I. Encapsulation of Carbon Nanotubes by Self Assembling Peptide Amphiphiles. *Langmuir* **2005**, *21*, 4705−4709.

(13) Iglesias, D.; Melchionna, M. Enter the Tubes: Carbon Nanotube Endohedral Catalysis. *Catalysts* **2019**, *9*, 128.

(14) Yanagi, K.; Iakoubovskii, K.; Matsui, H.; Matsuzaki, H.; Okamoto, H.; Miyata, Y.; Maniwa, Y.; Kazaoui, S.; Minami, N.; Kataura, H. Photosensitive Function of Encapsulated Dye in Carbon Nanotubes. *J. Am. Chem. Soc.* **2007**, *129*, 4992−4997.

(15) van Bezouw, S.; Arias, D. H.; Ihly, R.; Cambré, S.; Ferguson, A. J.; Campo, J.; Johnson, J. C.; Defillet, J.; Wenseleers, W.; Blackburn, J. L. Diameter Dependent Optical Absorption and Excitation Energy Transfer from Encapsulated Dye Molecules toward Single Walled Carbon Nanotubes. *ACS Nano* **2018**, *12*, 6881−6894.

(16) Cambré, S.; Campo, J.; Beirnaert, C.; Verlackt, C.; Cool, P.; Wenseleers, W. Asymmetric Dyes Align inside Carbon Nanotubes to Yield a Large Nonlinear Optical Response. *Nat. Nanotechnol.* **2015**, *10*, 248−252.

(17) Murakami, N.; Miyake, H.; Tajima, T.; Nishikawa, K.; Hirayama, R.; Takaguchi, Y. Enhanced Photosensitized Hydrogen Production by Encapsulation of Ferrocenyl Dyes into Single Walled Carbon Nanotubes. *J. Am. Chem. Soc.* **2018**, *140*, 3821−3824.

(18) Poudel, Y. R.; Li, W. Synthesis, Properties, and Applications of Carbon Nanotubes Filled with Foreign Materials: A Review. *Mater. Today Phys.* **2018**, *7*, 7−34.

(19) Streit, J.; Snyder, C. R.; Campo, J.; Zheng, M.; Simpson, J. R.; Hight Walker, A. R.; Fagan, J. A. Alkane Encapsulation Induces Strain in Small Diameter Single Wall Carbon Nanotubes. *J. Phys. Chem. C* **2018**, *122*, 11577−11585.

(20) Ma, X.; Cambré, S.; Wenseleers, W.; Doorn, S. K.; Htoon, H. Quasi Phase Transition in a Single File of Water Molecules Encapsulated in (6,5) Carbon Nanotubes Observed by Temper

ature Dependent Photoluminescence Spectroscopy. *Phys. Rev. Lett.* **2017**, *118*, 027402.
(21) Cambré, S.; Wenseleers, W. Separation and Diameter Sorting of Empty (End Capped) and Water Filled (Open) Carbon Nano tubes by Density Gradient Ultracentrifugation. *Angew. Chem., Int. Ed.* **2011**, *50*, 2764−2768.
(22) Köfinger, J.; Hummer, G.; Dellago, C. Single File Water in Nanopores. *Phys. Chem. Chem. Phys.* **2011**, *13*, 15403−15417.
(23) Maniwa, Y.; Kataura, H.; Abe, M.; Udaka, A.; Suzuki, S.; Achiba, Y.; Kira, H.; Matsuda, K.; Kadowaki, H.; Okabe, Y. Ordered Water inside Carbon Nanotubes: Formation of Pentagonal to Octagonal Ice Nanotubes. *Chem. Phys. Lett.* **2005**, *401*, 534−538.
(24) Takaiwa, D.; Hatano, I.; Koga, K.; Tanaka, H. Phase Diagram of Water in Carbon Nanotubes. *Proc. Natl. Acad. Sci. U. S. A.* **2008**, *105*, 39−43.
(25) Agrawal, K. V.; Shimizu, S.; Drahushuk, L. W.; Kilcoyne, D.; Strano, M. S. Observation of Extreme Phase Transition Temperatures of Water Confined inside Isolated Carbon Nanotubes. *Nat. Nanotechnol.* **2017**, *12*, 267.
(26) Majumder, M.; Chopra, N.; Andrews, R.; Hinds, B. J. Enhanced Flow in Carbon Nanotubes. *Nature* **2005**, *438*, 44−44.
(27) Holt, J. K.; Park, H. G.; Wang, Y.; Stadermann, M.; Artyukhin, A. B.; Grigoropoulos, C. P.; Noy, A.; Bakajin, O. Fast Mass Transport through Sub 2 Nanometer Carbon Nanotubes. *Science* **2006**, *312*, 1034−1037.
(28) Goh, K.; Chen, Y. Controlling Water Transport in Carbon Nanotubes. *Nano Today* **2017**, *14*, 13−15.
(29) Mikami, F.; Matsuda, K.; Kataura, H.; Maniwa, Y. Dielectric Properties of Water inside Single Walled Carbon Nanotubes. *ACS Nano* **2009**, *3*, 1279−1287.
(30) Nakamura, Y.; Ohno, T. Ferroelectric Mobile Water. *Phys. Chem. Chem. Phys.* **2011**, *13*, 1064−1069.
(31) Velioğlu, S.; Karahan, H. E.; Goh, K.; Bae, T. H.; Chen, Y.; Chew, J. W. Metallicity Dependent Ultrafast Water Transport in Carbon Nanotubes. *Small* **2020**, *16*, 1907575.
(32) Das, A.; Jayanthi, S.; Deepak, H. S. M. V.; Ramanathan, K. V.; Kumar, A.; Dasgupta, C.; Sood, A. K. Single File Diffusion of Confined Water inside Swnts: An Nmr Study. *ACS Nano* **2010**, *4*, 1687−1695.
(33) Kyakuno, H.; Matsuda, K.; Yahiro, H.; Inami, Y.; Fukuoka, T.; Miyata, Y.; Yanagi, K.; Maniwa, Y.; Kataura, H.; Saito, T.; et al. Confined Water inside Single Walled Carbon Nanotubes: Global Phase Diagram and Effect of Finite Length. *J. Chem. Phys.* **2011**, *134*, 244501.
(34) Cambré, S.; Santos, S. M.; Wenseleers, W.; Nugraha, A. R.; Saito, R.; Cognet, L.; Lounis, B. Luminescence Properties of Individual Empty and Water Filled Single Walled Carbon Nanotubes. *ACS Nano* **2012**, *6*, 2649−2655.
(35) Li, H.; Gordeev, G.; Garrity, O.; Peyyety, N. A.; Selvasundaram, P. B.; Dehm, S.; Krupke, R.; Cambré, S.; Wenseleers, W.; Reich, S.; et al. Separation of Specific Single Enantiomer Single Wall Carbon Nanotubes in the Large Diameter Regime. *ACS Nano* **2020**, *14*, 948−963.
(36) Li, H.; Gordeev, G.; Garrity, O.; Reich, S.; Flavel, B. S. Separation of Small Diameter Single Walled Carbon Nanotubes in One to Three Steps with Aqueous Two Phase Extraction. *ACS Nano* **2019**, *13*, 2567−2578.
(37) Nish, A.; Hwang, J. Y.; Doig, J.; Nicholas, R. J. Highly Selective Dispersion of Single Walled Carbon Nanotubes Using Aromatic Polymers. *Nat. Nanotechnol.* **2007**, *2*, 640.
(38) Samanta, S. K.; Fritsch, M.; Scherf, U.; Gomulya, W.; Bisri, S. Z.; Loi, M. A. Conjugated Polymer Assisted Dispersion of Single Wall Carbon Nanotubes: The Power of Polymer Wrapping. *Acc. Chem. Res.* **2014**, *47*, 2446−2456.
(39) Graf, A.; Zakharko, Y.; Schießl, S. P.; Backes, C.; Pfohl, M.; Flavel, B. S.; Zaumseil, J. Large Scale, Selective Dispersion of Long Single Walled Carbon Nanotubes with High Photoluminescence Quantum Yield by Shear Force Mixing. *Carbon* **2016**, *105*, 593−599.
(40) Jakubka, F.; Schießl, S. P.; Martin, S.; Englert, J. M.; Hauke, F.; Hirsch, A.; Zaumseil, J. Effect of Polymer Molecular Weight and Solution Parameters on Selective Dispersion of Single Walled Carbon Nanotubes. *ACS Macro Lett.* **2012**, *1*, 815−819.
(41) Liang, S.; Li, H.; Flavel, B. S.; Adronov, A. Effect of Single Walled Carbon Nanotube (SWCNT) Composition on Polyfluorene Based Swcnt Dispersion Selectivity. *Chem. Eur. J.* **2018**, *24*, 9799−9806.
(42) Bindl, D. J.; Safron, N. S.; Arnold, M. S. Dissociating Excitons Photogenerated in Semiconducting Carbon Nanotubes at Polymeric Photovoltaic Heterojunction Interfaces. *ACS Nano* **2010**, *4*, 5657−5664.
(43) Avery, A. D.; Zhou, B. H.; Lee, J.; Lee, E. S.; Miller, E. M.; Ihly, R.; Wesenberg, D.; Mistry, K. S.; Guillot, S. L.; Zink, B. L.; et al. Tailored Semiconducting Carbon Nanotube Networks with Enhanced Thermoelectric Properties. *Nat. Energy* **2016**, *1*, 16033.
(44) Brady, G. J.; Joo, Y.; Wu, M. Y.; Shea, M. J.; Gopalan, P.; Arnold, M. S. Polyfluorene Sorted, Carbon Nanotube Array Field Effect Transistors with Increased Current Density and High on/Off Ratio. *ACS Nano* **2014**, *8*, 11614−11621.
(45) Schneider, S.; Lefebvre, J.; Diercks, N. J.; Berger, F. J.; Lapointe, F. o.; Schleicher, J.; Malenfant, P. R.; Zaumseil, J. Phenanthroline Additives for Enhanced Semiconducting Carbon Nanotube Dispersion Stability and Transistor Performance. *ACS Appl. Nano Mater.* **2020**, *3*, 12314−12324.
(46) Statz, M.; Schneider, S.; Berger, F. J.; Lai, L.; Wood, W. A.; Abdi Jalebi, M.; Leingang, S.; Himmel, H. J. r.; Zaumseil, J.; Sirringhaus, H. Charge and Thermoelectric Transport in Polymer Sorted Semiconducting Single Walled Carbon Nanotube Networks. *ACS Nano* **2020**, *14*, 15552−15565.
(47) Wieland, L.; Li, H.; Rust, C.; Chen, J.; Flavel, B. S. Carbon Nanotubes for Photovoltaics: From Lab to Industry. *Adv. Energy Mater.* **2021**, *11*, 2002880.
(48) Shea, M. J.; Mehlenbacher, R. D.; Zanni, M. T.; Arnold, M. S. Experimental Measurement of the Binding Configuration and Coverage of Chirality Sorting Polyfluorenes on Carbon Nanotubes. *J. Phys. Chem. Lett.* **2014**, *5*, 3742−3749.
(49) Li, H.; Gordeev, G.; Wasserroth, S.; Chakravadhanula, V. S. K.; Neelakandhan, S. K. C.; Hennrich, F.; Jorio, A.; Reich, S.; Krupke, R.; Flavel, B. S. Inner and Outer Wall Sorting of Double Walled Carbon Nanotubes. *Nat. Nanotechnol.* **2017**, *12*, 1176−1182.
(50) Araujo, P. T.; Doorn, S. K.; Kilina, S.; Tretiak, S.; Einarsson, E.; Maruyama, S.; Chacham, H.; Pimenta, M. A.; Jorio, A. Third and Fourth Optical Transitions in Semiconducting Carbon Nanotubes. *Phys. Rev. Lett.* **2007**, *98*, 067401.
(51) Maultzsch, J.; Telg, H.; Reich, S.; Thomsen, C. Radial Breathing Mode of Single Walled Carbon Nanotubes: Optical Transition Energies and Chiral Index Assignment. *Phys. Rev. B: Condens. Matter Mater. Phys.* **2005**, *72*, 205438.
(52) Abraham, M. J.; Murtola, T.; Schulz, R.; Páll, S.; Smith, J. C.; Hess, B.; Lindahl, E. Gromacs: High Performance Molecular Simulations through Multi Level Parallelism from Laptops to Supercomputers. *SoftwareX* **2015**, *1*, 19−25.
(53) Martínez, L.; Andrade, R.; Birgin, E. G.; Martínez, J. M. Packmol: A Package for Building Initial Configurations for Molecular Dynamics Simulations. *J. Comput. Chem.* **2009**, *30*, 2157−2164.
(54) Wang, J.; Wang, W.; Kollman, P. A.; Case, D. A. Automatic Atom Type and Bond Type Perception in Molecular Mechanical Calculations. *J. Mol. Graphics Modell.* **2006**, *25*, 247−260.
(55) Bayly, C. I.; Cieplak, P.; Cornell, W.; Kollman, P. A. A Well Behaved Electrostatic Potential Based Method Using Charge Restraints for Deriving Atomic Charges: The Resp Model. *J. Phys. Chem.* **1993**, *97*, 10269−10280.
(56) González, M. A.; Abascal, J. L. A Flexible Model for Water Based on Tip4p/2005. *J. Chem. Phys.* **2011**, *135*, 224516.
(57) Dalla Bernardina, S.; Paineau, E.; Brubach, J. B.; Judeinstein, P.; Rouziere, S.; Launois, P.; Roy, P. Water in Carbon Nanotubes: The Peculiar Hydrogen Bond Network Revealed by Infrared Spectroscopy. *J. Am. Chem. Soc.* **2016**, *138*, 10437−10443.

(58) Chakraborty, S.; Kumar, H.; Dasgupta, C.; Maiti, P. K. Confined Water: Structure, Dynamics, and Thermodynamics. *Acc. Chem. Res.* **2017**, *50*, 2139−2146.
(59) Campo, J.; Cambré, S.; Botka, B.; Obrzut, J.; Wenseleers, W.; Fagan, J. A. Optical Property Tuning of Single Wall Carbon Nanotubes by Endohedral Encapsulation of a Wide Variety of Dielectric Molecules. *ACS Nano* **2021**, *15*, 2301−2317.
(60) Silvera Batista, C. A.; Zheng, M.; Khripin, C. Y.; Tu, X.; Fagan, J. A. Rod Hydrodynamics and Length Distributions of Single Wall Carbon Nanotubes Using Analytical Ultracentrifugation. *Langmuir* **2014**, *30*, 4895−4904.
(61) Kanai, Y.; Grossman, J. C. Role of Semiconducting and Metallic Tubes in P3ht/Carbon Nanotube Photovoltaic Heterojunctions: Density Functional Theory Calculations. *Nano Lett.* **2008**, *8*, 908−912.
(62) Wang, H.; Hsieh, B.; Jiménez Osés, G.; Liu, P.; Tassone, C. J.; Diao, Y.; Lei, T.; Houk, K. N.; Bao, Z. Solvent Effects on Polymer Sorting of Carbon Nanotubes with Applications in Printed Electronics. *Small* **2015**, *11*, 126−133.
(63) Császár, A. G.; Mátyus, E.; Szidarovszky, T.; Lodi, L.; Zobov, N. F.; Shirin, S. V.; Polyansky, O. L.; Tennyson, J. First Principles Prediction and Partial Characterization of the Vibrational States of Water up to Dissociation. *J. Quant. Spectrosc. Radiat. Transfer* **2010**, *111*, 1043−1064.
(64) Byl, O.; Liu, J. C.; Wang, Y.; Yim, W. L.; Johnson, J. K.; Yates, J. T. Unusual Hydrogen Bonding in Water Filled Carbon Nanotubes. *J. Am. Chem. Soc.* **2006**, *128*, 12090−12097.
(65) Buch, V.; Devlin, J. P., Eds. *Water in Confining Geometries*; Springer Science & Business Media: Berlin Heidelberg, 2013.
(66) Alexiadis, A.; Kassinos, S. Molecular Simulation of Water in Carbon Nanotubes. *Chem. Rev.* **2008**, *108*, 5014−5034.
(67) Martí, J.; Gordillo, M. Effects of Confinement on the Vibrational Spectra of Liquid Water Adsorbed in Carbon Nanotubes. *Phys. Rev. B: Condens. Matter Mater. Phys.* **2001**, *63*, 165430.
(68) Ellison, M. D.; Good, A. P.; Kinnaman, C. S.; Padgett, N. E. Interaction of Water with Single Walled Carbon Nanotubes: Reaction and Adsorption. *J. Phys. Chem. B* **2005**, *109*, 10640−10646.
(69) Chen, J.; Wan, L.; Li, H.; Yan, J.; Ma, J.; Sun, B.; Li, F.; Flavel, B. S. A Polymer/Carbon Nanotube Ink as a Boron Dopant/Inorganic Passivation Free Carrier Selective Contact for Silicon Solar Cells with over 21% Efficiency. *Adv. Funct. Mater.* **2020**, *30*, 2004476.
(70) Chen, J.; Tune, D. D.; Ge, K.; Li, H.; Flavel, B. S. Front and Back Junction Carbon Nanotube Silicon Solar Cells with an Industrial Architecture. *Adv. Funct. Mater.* **2020**, *30*, 2000484.
(71) Cambré, S.; Schoeters, B.; Luyckx, S.; Goovaerts, E.; Wenseleers, W. Experimental Observation of Single File Water Filling of Thin Single Wall Carbon Nanotubes Down to Chiral Index (5, 3). *Phys. Rev. Lett.* **2010**, *104*, 207401.
(72) Wenseleers, W.; Cambré, S.; Čulin, J.; Bouwen, A.; Goovaerts, E. Effect of Water Filling on the Electronic and Vibrational Resonances of Carbon Nanotubes: Characterizing Tube Opening by Raman Spectroscopy. *Adv. Mater.* **2007**, *19*, 2274−2278.
(73) Qu, H.; Rayabharam, A.; Wu, X.; Wang, P.; Li, Y.; Fagan, J.; Aluru, N. R.; Wang, Y. Selective Filling of N Hexane in a Tight Nanopore. *Nat. Commun.* **2021**, *12*, 310.
(74) Baertsch, C. D.; Funke, H. H.; Falconer, J. L.; Noble, R. D. Permeation of Aromatic Hydrocarbon Vapors through Silicalite−Zeolite Membranes. *J. Phys. Chem.* **1996**, *100*, 7676−7679.
(75) Gaulke, M.; Janissek, A.; Peyyety, N. A.; Alamgir, I.; Riaz, A.; Dehm, S.; Li, H.; Lemmer, U.; Flavel, B. S.; Kappes, M. M.; et al. Low Temperature Electroluminescence Excitation Mapping of Excitons and Trions in Short Channel Monochiral Carbon Nanotube Devices. *ACS Nano* **2020**, *14*, 2709−2717.
(76) Alam, A.; Dehm, S.; Hennrich, F.; Zakharko, Y.; Graf, A.; Pfohl, M.; Hossain, I. M.; Kappes, M. M.; Zaumseil, J.; Krupke, R.; et al. Photocurrent Spectroscopy of Dye Sensitized Carbon Nanotubes. *Nanoscale* **2017**, *9*, 11205−11213.
(77) Pfohl, M.; Glaser, K.; Graf, A.; Mertens, A.; Tune, D. D.; Puerckhauer, T.; Alam, A.; Wei, L.; Chen, Y.; Zaumseil, J.; et al. Probing the Diameter Limit of Single Walled Carbon Nanotubes in Swcnt: Fullerene Solar Cells. *Adv. Energy Mater.* **2016**, *6*, 1600890.
(78) Brady, G. J.; Joo, Y.; Singha Roy, S.; Gopalan, P.; Arnold, M. S. High Performance Transistors Via Aligned Polyfluorene Sorted Carbon Nanotubes. *Appl. Phys. Lett.* **2014**, *104*, 083107.
(79) Joo, Y.; Brady, G. J.; Kanimozhi, C.; Ko, J.; Shea, M. J.; Strand, M. T.; Arnold, M. S.; Gopalan, P. Polymer Free Electronic Grade Aligned Semiconducting Carbon Nanotube Array. *ACS Appl. Mater. Interfaces* **2017**, *9*, 28859−28867.
(80) Pfohl, M.; Glaser, K.; Ludwig, J.; Tune, D. D.; Dehm, S.; Kayser, C.; Colsmann, A.; Krupke, R.; Flavel, B. S. Performance Enhancement of Polymer Free Carbon Nanotube Solar Cells Via Transfer Matrix Modeling. *Adv. Energy Mater.* **2016**, *6*, 1501345.